

Aeromagnetic Investigation of the Ibuji, Southwestern, Nigeria

Bamisaiye, O.A.

Department of Applied Geology, Federal University of Technology, P.M.B 705, Akure, Nigeria.

Corresponding E-mail: adunseyi@gmail.com

Abstract

Ibuji area, southwestern Nigeria, has been speculated to play host to some important minerals. This study provides an overview of both surface and subsurface lithology and structure through aeromagnetic data analysis and interpretation with field verification. The aeromagnetic data shows a striking pattern in the magnetic characteristics of each lithology. This was used in deducing the depth, shape and dip of each rock type. Edges of the interpreted structural zones were delineated using Source Edge Detector (SED) techniques. The Standard Euler Deconvolution tool was used to estimate the depth of structures. An NNE-SSW trending fault with more than three hundred meters in length is one of the major structures that has affected this area and is related to the regional tectonic stress field. Since most mineralization are confined within structures, this fault and the hinges of the various folds, identified in this area, have been earmarked as favourable sites for mineral prospecting. The interpretation of the basement tectonics revealed a major fracture zone close to the contact between the migmatite and quartzite at the northwestern part of the study area and has been highlighted as one of the sites for geochemical investigation.

Keywords: Aeromagnetic data, Euler Deconvolution, Subsurface structures, Lithology, Basement.

Introduction

This research is aimed at improving the understanding of the gross structure and lithology of the area around southwestern Nigeria as part of the preliminary mineral exploration studies in the area. The study area covers a few towns in Ekiti State, Southwestern Nigeria and falls within latitudes 07°25'00"N to 07°30'00"N and longitudes 05°00'00"E to 05°05'00"E (Figure 1a) respectively. The study area falls within Ilesha Schist Belt (Figure 1), with the presence of some enthralling structural features and lithologies which are host economically important sites. Gold is currently being mined in some parts of the Schist belt with some industrial minerals and gemstones such as feldspar, mica, garnet, tourmaline, and beryl. These Upper Proterozoic supercrustal rocks generally referred to as the Schist Belts in Nigeria (Figure 1c) are highly folded and like some other metamorphic fold belts in the world (e.g. the Brasilia fold belt, the Sukhothai fold belt in Thailand; the Xiaoqinling-Xiong'er shan region in Central China; the Tombstone Gold Belt in Canada etc. are mineralized (Grove et al., 2003). Tectonic control on ore fluid deposition and concentration in all the belts is an established fact that has significantly improved the understanding of ore fluid genesis (Fagbohun et al., 2020). However, the source of mineralization fluid in these belts is still controversial, metamorphism and/or magmatic-hydrothermal fluids are suggested (Nguimatsia et al., 2017). The northern parts of this area (Figure 1a) are dominated by structurally-controlled mineral deposits (Ijero and Aramoko (Tin, Tantalum-niobium, lithium, gold and gemstones (Ale et al. 2014))) and its pertinent to determine if the mineralization extends to the southern parts i.e. the Ibuji

area. Previous studies in this area include the mapping and characterization of alteration zones which coincides with some of the gold mining sites and possible orogenic gold prospective areas in Imesi, Iwoye to Erin-Ijesha area all in the northern parts of the Ilesha schist belt (Akinlalu, 2023). Nkiru et al., 2018 evaluated the economic potentials of parts of the Ilesha schist belt and highlighted the areas of possible mineralization sites around Ondo, Ife, Ifewara and Odigbo. Elueze (1982) had earlier identified various ore minerals in the Ilesha rocks and described their metallographic properties. The study area falls within the southern parts of most of these previous studies. The aeromagnetic interpretation was compared to the existing structural and geological interpretation of the area. The main rock types in the area are granite, quartzite, migmatite and granite gneiss.

Aeromagnetic data interpretation for both subsurface lithologic contact and structural delineation had been applied severally for tectonic evolutionary studies (Hassanein and Soliman 2008; Ibraheem 2019; Ishola et al., 2020) and demarcation of structurally controlled mineralization (Ugbor et al., 2020; Zhang et al., 2020).

Geological Setting

The study area is part of the Nigeria Basement Complex, which lies between the West African and Congo Craton. The Nigerian Basement Complex consists of Precambrian rocks with infolded Schist Belts (Rahaman (1988)). The geology of Ibuji area can be subdivided into migmatite – gneiss complex, which is dominated by deformed and metamorphosed sedimentary series with associated minor igneous rock intrusions; the Pan African granitoids and the undeformed and basic dykes.

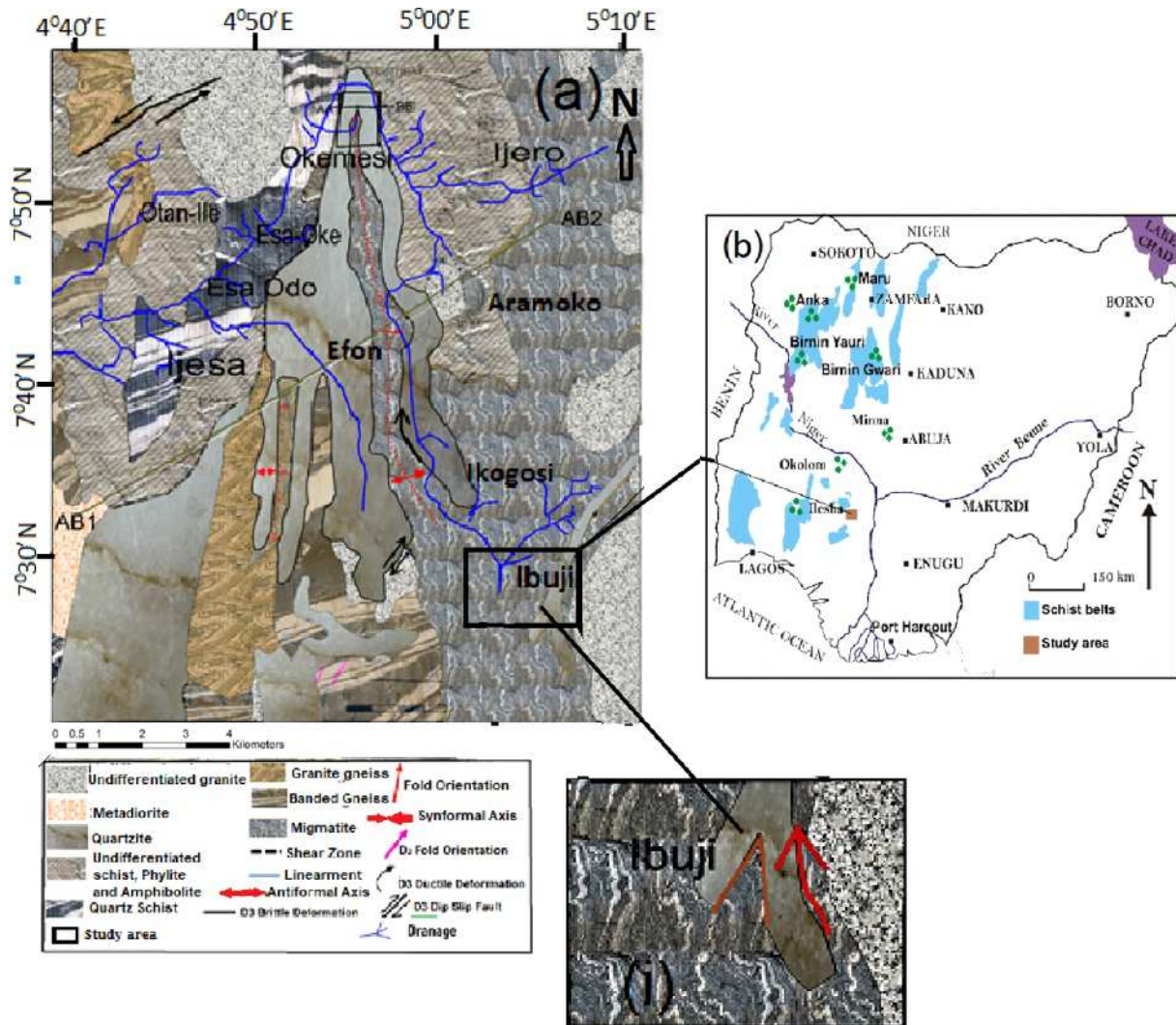


Fig. 1: (a) A generalized geologic map the Ilesha Schist Belt showing the mapped area with some locations referred to in the text (modified after Odeyemi, 1985). (b) the map of Nigeria showing the Schist Belt (modified after Andongma et al., 2020) and inset (i) showing brittle (brown triangle) and ductile (red arrow) deformation.

The metamorphosed sedimentary and volcanic rocks are generally referred to as the Schist Belt and are also infolded into the migmatite- gneiss complex. The study area is part of the NNE-SSW trending Ilesha Schist Belt and Ifewara shear zone (Figure 1c), which is lithologically made up of quartzites, schists and amphibolites which play host to many of the economic deposits (Olomo et al., 2022).

Foliation exhibited by rocks in this region is likely tectonic in origin (Odeyemi 1999). Obliteration of earlier deformation imprints by later deformations was also reported by Odeyemi, (1999). Anifowose (2004) reported the dominant NE-SW foliation trend within the Ilesha schist belt. The Nigeria Basement Complex has suffered at least two deformation episodes, namely the first deformational episode (D1) and the second

deformational episode (D2) (Boesse and Ocan, 1992). The first deformation episode (D1) is characterized by tight to isoclinal folds while the second deformation episode (D2) is characterized by more open folds of varying style and a vertical NE-SW trending fault (Boesse and Ocan, 1992). Oluyide (1988) gave evidence that earlier structures within the Schist Belt (Figure 1c), have been completely obliterated by the latter ones except in isolated places.

Dada (2006) classified the Nigerian Basement rocks into four lithologic units. These are:

- I. Migmatite-Gneiss-Quartzite Complex;
- II. The Schist Belts
- III. Pan African Granitoids and;
- IV. Unmetamorphosed minor acid and basic rocks

Methodology

Acquisition, Processing and Presentation of data

The aeromagnetic data used for this investigation was provided by the Nigeria Geological Survey. The data were acquired between 2004 and 2006 during a Fugro Airborne survey with a 3x-Scintrex CS3 Cesium Vapor magnetometer. Operated at 80 m sensor mean terrain clearance and 0.1s (~ 7m) magnetic data recording interval. The central part of the area under investigation has a 11.279° inclination angle and -1.728° declination angle.. This is because the inclination of the Earth's magnetic field in the study area is -11.279° and, consequently, the total field image, as recorded, shows extreme anomalous asymmetry. The asymmetry has been removed by the reduction to the equator process. The low latitude anomalies, were resolved by applying the Reduction to the Equator (RTE) using the Geosoft package software, Oasis Montaj ®TM v.6.4.2. Cultural noise (which might be due to the presence of railway lines and electric power lines) was removed by Butterworth filtering.

Also, the deep-seated noise (regional) in the data was removed by separation from the Total Magnetic Field Intensity (TMI) data. The resultant data were analysed using ArcGIS (version 10.2). The signal-to-noise ratio of the raw data was increased by removing the noise aspect with 100 m upward continuation filtering.

For instance, in areas which are close to the equator where the rock's predominant magnetisation is by induction, without significant permanent magnetisation in a direction other than that of the Earth's field, the anomalies are reduced to the equator for maps and images. The signal-to-noise ratio of the raw data was increased by removing the noise aspect with 100 m upward continuation filtering.

The basic concepts of the magnetic method have been adequately explained in many textbooks (e.g. Blakely and Simpson 1986; Blakely 1996; Kearey et al., 2003). All necessary corrections applied to the raw data and the resultant maps (RMA) were further enhanced to improve the signal strength. The signal enhancement techniques applied include; Total Horizontal Derivative (THD), Second Vertical Derivative (SVD) and 3-D standard Euler deconvolution. A brief discussion on the theory and the attributes of the different correction and enhancement techniques is stated below.

Two- dimensional (2-D) geologic profiles of the

subsurface were produced with GM- SYS, a Geosoft software. The method used for calculating the magnetic response was based on the algorithms described in Wen and Bevis (1987). The Euler deconvolution technique (Reid et al. 1990; Amigun and Adelus 2013; Amigun et al., 2012) is preferred over the profile techniques such as Peters (1949) method (half slope) because the source magnetization direction is not predetermined. This has prompted its application in this study for the determination of depths to magnetic source using the analytical signal amplitude. Where local minima distance and the depth to source directly correlates. A structural Index of 0.5, a window size of 15 and a maximum distance of 250 were used to generate the 3D Euler Deconvolution.

This makes the resultant maps and images easier to interpret, especially in areas with notable magnetic inclinations. Subsequently, the data were subjected to interpretation by identifying the contacts and classifying the lithologies and lineaments. Areas of negative magnetic anomalies (corresponding at low magnetic latitudes to higher magnetic susceptibility) and low magnetic relief zones are surrounded by high magnetic relief zones.

A digitized aeromagnetic data of the Ibuti area which fall in sheet 264 was processed for interpretation purposes. The geologic map of the area was included to serve as a check for the interpreted aeromagnetic data. Ground truthing of the features delineated from the interpretation of the image was carried out during the field exercise. The necessary field data acquisitions such as the rock samples collection, measurements of orientation of structures and other observations were carried out during geologic field mapping. The field data were collected based on the followings: proper observation, identification of the rocks, collection of structural data by observation of rock disposition and other structural elements and correlating the results of the processed data to what is seen on the ground.

Results

The Total Magnetic Intensity (TMI) image produced for this area is a colour-coded image which illuminates the northern and the cast shadow on the southern side. This illumination resulted in the NE-SW strike display in the study area (Figure 2). The difference between the TMI and the Residual in Figure 2 may not be too significant because the regional anomaly effect had been filtered off.

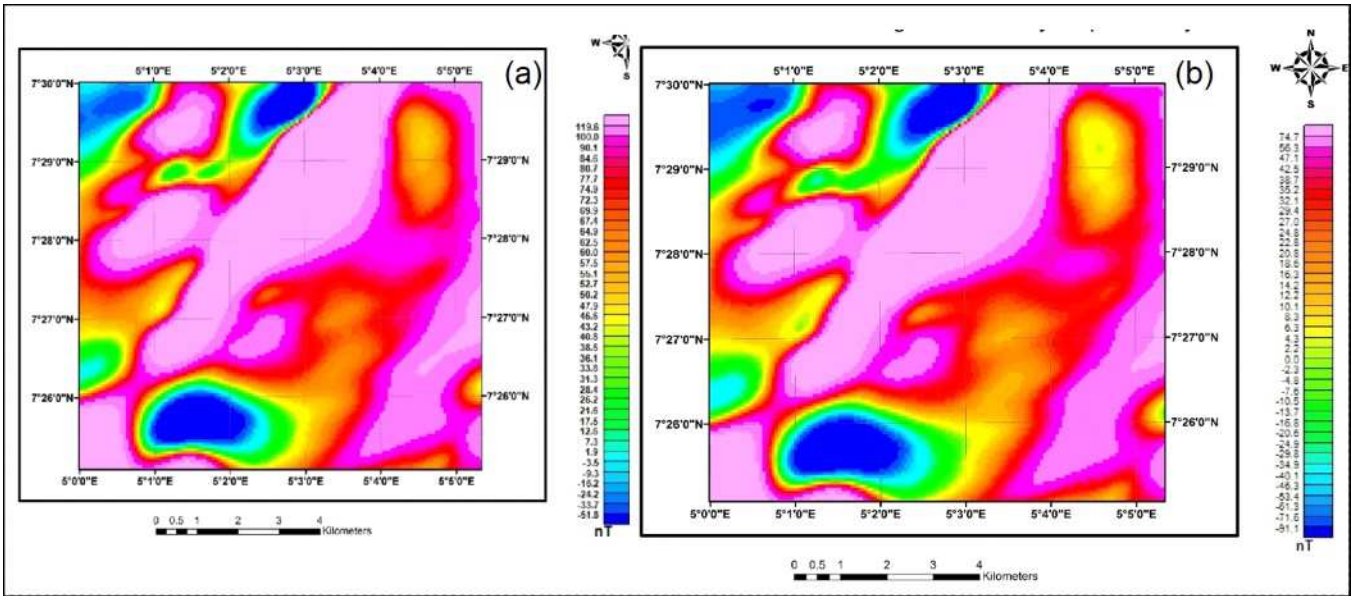


Fig. 2: (a) Total Magnetic Intensity reduced to the Equator for enhanced magnetic significance. (b) Residual Magnetic Anomaly (RMA) indicates dominant magnetic anomaly trends in the NE-SW direction.

Interpretation of aeromagnetic data was performed on the magnetic data set that had been reduced to the equator ((RTE) Figure 2a). The residual magnetic anomaly (RMA) is also presented as a colour-shaded map below (Figure 2b). The Total Horizontal Derivative was carried out to further enhance the magnetic anomalies (Figure 3a) and articulate the dominant magnetic anomaly trends, which are in the NE-SW direction. These anomalies correspond respectively to

magnetic susceptibility contrasts between the various lithologies of the crystalline basement rocks in the study area. Areas of negative magnetic anomalies (corresponding at low magnetic latitudes to higher magnetic susceptibility) and low magnetic relief zones are surrounded encapsulated by high magnetic relief zones. The magnetic intensity of the THD field ranges from -91.1 nT to 74.7 nT.

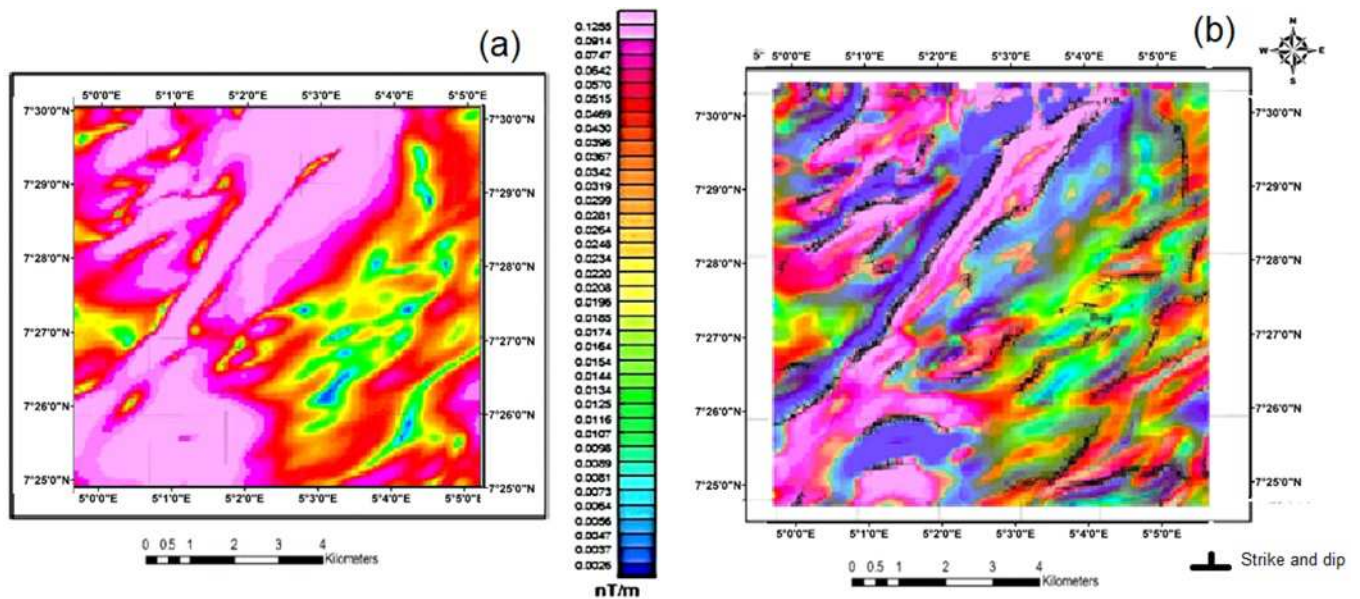


Fig. 3: (a) Total Horizontal Derivative (THD). (b) the THD map overlain on the Second Vertical Derivative (SVD).

The results of the total horizontal derivative (THD) technique applied to the RTE data are presented as a colour-shaded relief map (Figure 3a). The THD results

of the RTE give contact locations that are continuous, thin and curvilinear (Figure 3a). The maps show major contacts in the NE-SW, E-W directions which

correspond to geological contact zones with a moderate magnetic susceptibility difference on the RTE THD. The amplitudes of the gradient are up to 0.1255 nT/m on the RTE THD map.

Similarly, the result of the second vertical derivative (SVD) analysis on the RTE data is presented as colour-shaded relief maps overlain by contour lines (Figure 3b). The SVD technique does not usually result in displaced contacts because it does not require the assumptions in the THD technique. As a result of this, the final location of contacts is estimated using the following considerations; where the THD contacts are isolated or non-continuous, the SVD contact location (Figure 3b) gives the best contact location (Oyeniyi et.al., 2022). In a similar manner, where the THD

contacts are either parallel to or slightly offset from the SVD contact location, the SVD contact gives the preferred contact location. The SVD maps show similarities with its corresponding THD map, and the locations of contacts are indicated by contour lines on the RMA SVD (Figure 3b). It is observed that the contact locations on the SVD maps also show better continuity than those on the THD maps. The extracted contacts from the SVD and THD maps are shown in Figure 5b. Sub-section of the south-eastern part of Ilesha schist belt shows the geology and evidence of D3 deformation around Ibuji area (Figure 4a). Figure 4b shows the existing geologic map while Figure 4c represents the extracted geologic contacts and structures interpreted from aeromagnetic data.

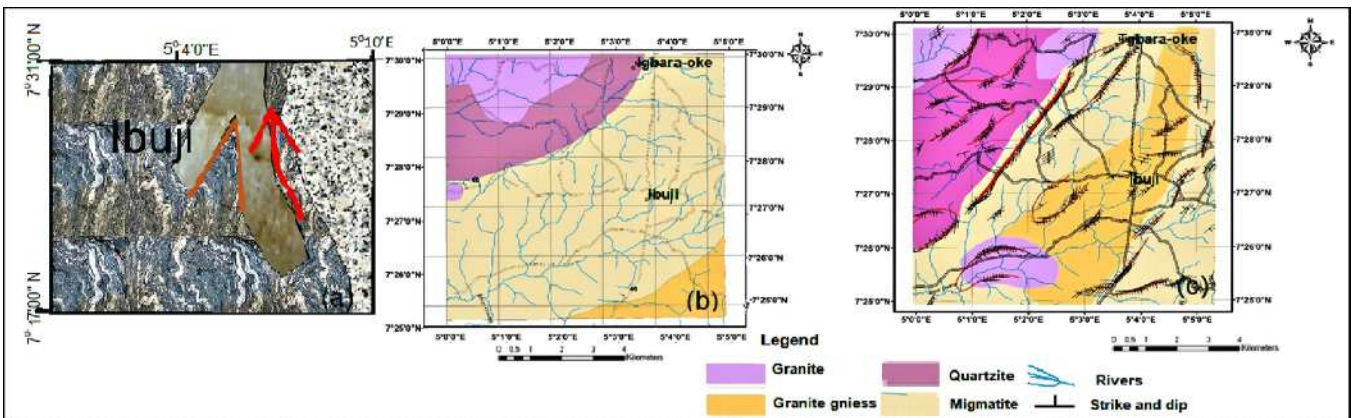


Fig. 4: (a) Part of the Ilesha schist belt showing the southeastern quartzite ridge that extends to Ibuji area and the early ductile (red arrow) and later brittle deformation (brown triangle) that characterized the D3 deformational episode. (b) is the existing geological map as represented at the surface, (c) is the geological map derived from the analysis and interpretation of the aeromagnetic data of the same area as represented at the subsurface.

The result of the analysis of Euler Deconvolution on the RMA data is presented as a colour-range symbol map in (Figure 5a) This analysis determines the anomalous position, depth, and base level for a specific magnetic source. Several structural index values were tried for the Euler analysis, a structural index of $N = 0$, representing a contact model, gave better clustering of the Euler solutions (Figure 5). The green and red points, which define depths greater than 300 m respectively, show the same consistent trends for the lithological contacts mapped by the THD and SVD results. In the central region, clusters of broken green and red coloured points suggest the presence of a major structure not previously mapped. The uniform depth of solutions in the major structural zones suggests the absence of vertical displacement within the zone (Bellier et.al., 1991), what can be inferred from this is a limb of a major fold. Figure 6b shows the result of the 3D analytical estimates of both horizontal and vertical source positions of a noise-

free magmatic anomaly overlaid with some of the observed lineaments related to the source of the magnetic anomaly at depth. The correlation of the interpreted structures and the rivers in the area (Figure 6a) reveals some correlation between the pattern of surface structural information and the structural trends at depth.

The geological field mapping of the study area was carried out in order to get a basic understanding of the geology of the study area and also serve as a check for the aeromagnetic data interpretation. Both were integrated for the production of a modified new geological map. The major rock types encountered in the field are described below.

Quartzite

Quartzite was encountered around Ogotun in Ekiti state,

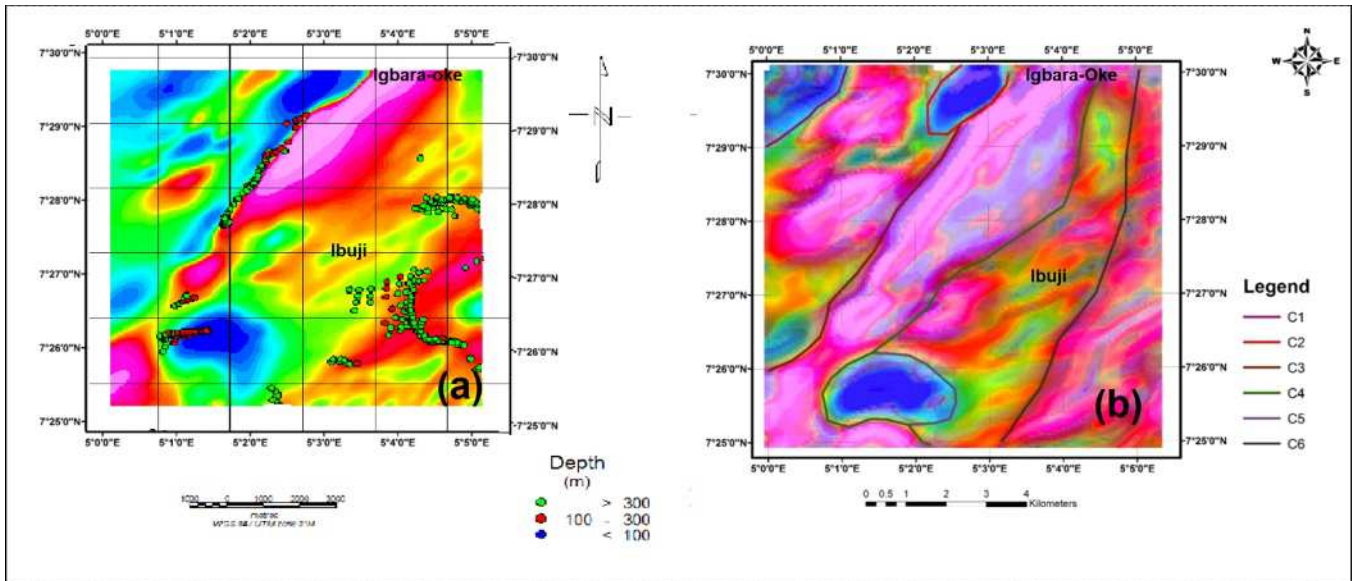


Fig. 5: (a) Euler Deconvolution overlaid on the RMA map shows the depth along the major Fault in the area. It indicates that the structures are deep-seated. (b) Geological Contacts extracted from the aeromagnetic analysis. These anomalies correspond respectively to magnetic susceptibility between the various lithologies and minerals of the crystalline basement rocks.

Aba Odua in Osun state, the major outcrops occur as high and elongated ridges. The quartzite is highly vegetated and weathered which made it difficult to acquire any measurement in some areas and this location includes the N, NW and NNW areas of the study map. The quartzite is diamagnetic with negative susceptibility and is not easily detected except when it is contaminated with other magnetic minerals.

Migmatite

Migmatites were encountered both in the northern and the southern parts of the mapped area. The migmatite occurs as stock in Igbara Odo in the northeastern part of the mapped area. Most of the mapped migmatite occurs as a low-lying outcrop ranging in textural characteristics from medium to coarse-grained. There is clear evidence of material flow during metamorphisms that affected the country rock, evidenced by folding. Structures like ptygmatic folds, microfolds, dykes and veins were observed on the outcrop; evidence of persistent recrystallization. These migmatites are coarse-grained. The presence of plagioclase in the thin section might signify an igneous origin or melt from an I-type granite melt. The outcrops are highly deformed and show attributes of plastic deformation i.e. the presence of folds and quartzofeldspathic veins.

Granitic Gneiss

The Granite Gneiss is heterogeneous, consisting of metamorphic and granitic portions with varying textural

characteristics. The mineralogy of the outcrop is characterized by felsic minerals such as quartz, and feldspar and also dark-coloured bands of minerals which are mostly biotite. The rock also displayed varieties of structural elements such as folds and faults.

Granite

The Granite occurs as a stock in most locations majority of the granite seen contains both mafic and felsic minerals of different compositions, the felsic minerals are mainly quartz and feldspar while the mafic minerals are mainly biotite. These granites are paramagnetic. The presence of ilmenite in the ppl in Figure 7N. A cross section and profiles over some of the rocks and rock contact is shown in Figure 7N (a and b).

Discussion

Based on the interpretation of the residual magnetic anomalies, the total horizontal derivative maps (Figure 3a), the second vertical derivative maps (Figure 3b) and the Euler map (5a), the main lithologies in the study area (Figure 5b), can be divided into seven main magnetic anomaly zones demarcated by six contact locations (C1, C2, C3, C4, C5, and C6). These Zones correlate with the existing geological map. The zone between C1 and C2 and C3 is dominated by quartzite, while the zone between C3 and C4 is made up of migmatite. However, the granite in the northwest (Figure 4) may not be as extensive at the subsurface as shown in the geological map. In a similar manner, the

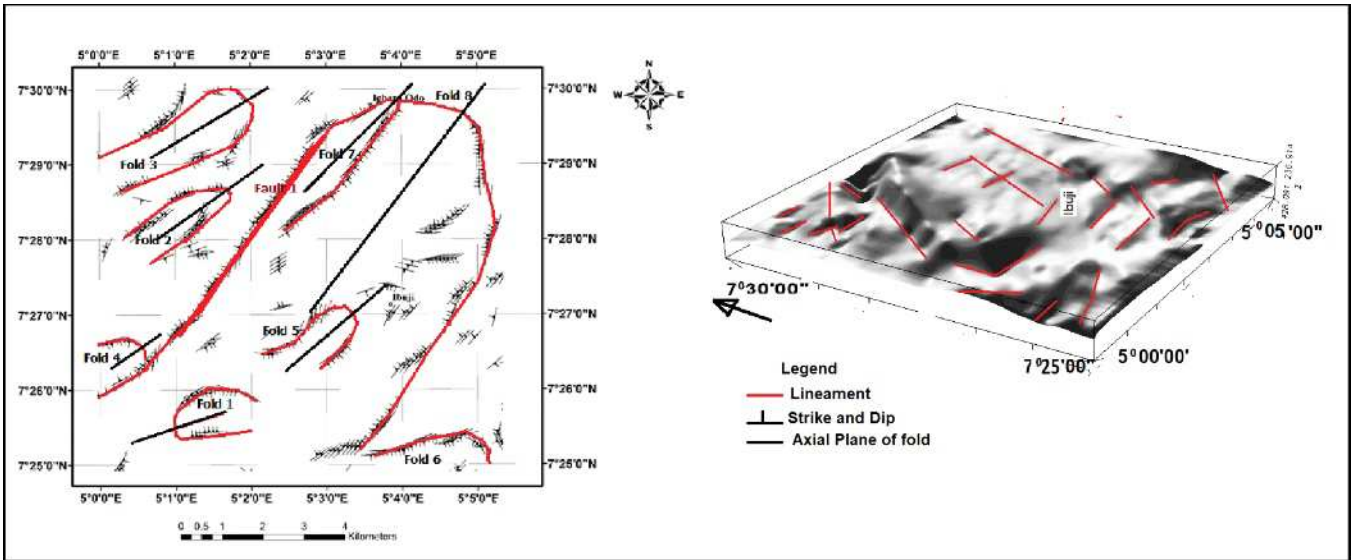


Fig. 6: (a) The structures extracted from aeromagnetic data analysis and overlaid on the surface drainage system to view the correlation (b) 3D model overlaid by Lineament map.

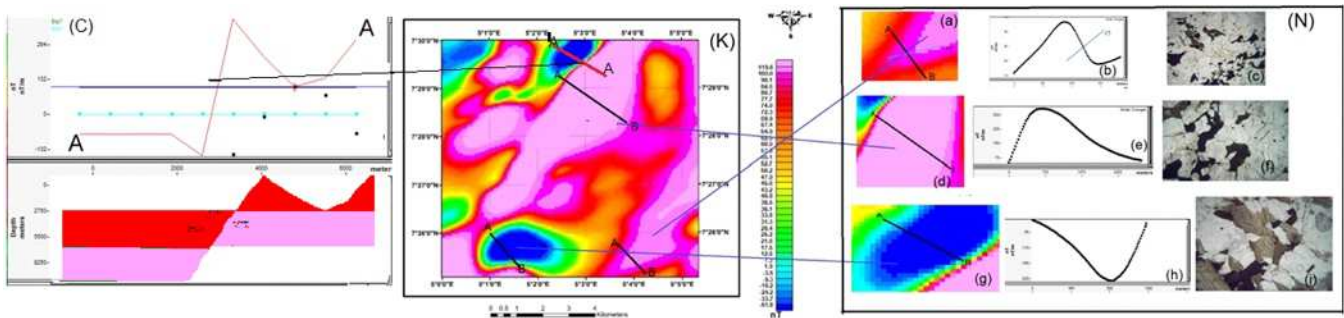


Fig.7: (C) Reveal a distinct contact that coincides with a fault plane represented by a sharp drop in magnetic intensity between 1A and A. (K) is the RMA map showing the profiles lines. N(a) profile AB was over the Migmatite terrain in the Southeastern part of the study. N (b) the magnetic profile of the shows a high to low positive anomaly. (c) shows the photomicrograph with of the Migmatite. N(d) shows Profile AB in a Migmatite-gneiss terrain at the Northwestern area of the RMA map. N(e) is the Magnetic Grid over the granitic terrain showing a smooth negative anomaly. N(f) shows the photomicrograph with ilmenite, quartz, and biotite under PPL. N(g) Traverse AB was over the Granitic terrain in the southwestern area of the RMA map. The magnetic profile N(h) of the area shows a smooth negative anomaly. The photomicrograph N(i) shows the minerals present in the rock.

lithologic contacts C4 and C5 derived from the magnetic map suggest that migmatite is not as extensive in the southwest and eastern part of the area as indicated in Figure 4a and 4b; while the granite gneiss in the southeastern part is extensive than indicated on the existing geologic map.

A traverse line AB (Figure 7(N)a) on the migmatite terrain in the southeastern part of the mapped area and the magnetic profile (Figure 7(N)b). The magnetic profile (Figure 7 (N)b) shows a high to low positive anomaly which coincides with the contact C5 between the migmatite and granite gneiss. The photomicrograph of migmatite (Figure 7(N)c) in the southeastern part of the map under Plane Polarised Light (PPL). The photomicrograph shows the presence of quartz and feldspar which are the lighter areas of the

photomicrograph. The mafic constituents are responsible for the high magnetic susceptibility. Basic rocks have a maximum magnetic susceptibility of about 0.12, the presence of basic minerals in migmatite could be responsible for this high positive magnetic anomaly.

Traverse AB (Figure 7K(d)) was also taken over the migmatite terrain in the central area of the study map the magnetic profile (Figure 7K(e)) of the area shows a smooth, broad positive anomaly also a sample was taken from this location which falls in the migmatite terrain, the photomicrograph viewed in Plane Polarised Light mode (Figure 7K(f)) shows the minerals present in the rock sample from the traverse area: Qtz = Quartz, Flds = Feldspar, Biot = Biotite and it can be inferred that the minerals present could be responsible for the moderately high magnetic intensity in the area.

Traverse AB (Figure 7K (g)) drawn over the Granitic terrain in the Northwest of the study area (Figure 7K(h)) shows a smooth, negative anomaly also a sample was taken from this location and it falls within the Granitic terrain, the photomicrograph (Figure 7K(i)) shows the minerals present in the rock sample taken from the traverse area which is Qtz = Quartz, Flds = Feldspar, Bio = Biotite. Out of the three prominent rocks in the area, the migmatite and granite have higher magnetic susceptibility and display stronger magnetic anomalies than quartzite.

Structures

Information obtained from the SED (Source Edge Detector) Map, 3D Euler Deconvolution map, SVD map, THD map and aeromagnetic profiles was used in producing a subsurface structural map of the study area. The overlay of the interpreted structures on the drainage system (Figure 7a) reveals a close correlation. On the 3D model (Figure 6a), the prominent and younger NNE-SSW and NE-SW trending lineaments cut across the shorter and older E-W and ESE-WNW lineaments. The E-W trending lineaments are likely relics of the D1 ductile deformational episode. The N-S to NNE-SSW lineaments belong to the D2 deformational episode. The NE-SW trending lineaments are part of the brittle/ductile D3 deformation. The cross-section (7(C)) reveals the geometry of the main fault in this area.

There are six deep geologic contact zones within the study area (Figure 5a). Contact C1, represents the contact between granite and quartzite in the NNW part of the map and C2 represents the contact between quartzite and granite also between the granite and migmatite in the Northern part of the study area, both contacts trends NNE-SSW, the depth of the C2 is between 100 - 300 m. C3 indicates the contact zone between the quartzite and migmatite in the central area of the map, trends in the NNE-SSW direction with a depth range of about 300 m. C4 shows the boundary between migmatite, granite gneiss and granite and trends NNE-SSW. C5 represents the boundary between migmatite, granite, and granite gneiss in the southern part of the study map and trends east-west. While, C6 signifies the contact between the migmatite and granite gneiss, trends NNE-SSE with a minimum depth of 300 m.

The SVD, THD, SED and the Euler Deconvolution maps were overlaid in order to delineate the major structures in the area. A major fault structure was identified within the study area which trends NE-SW

with a reverse/thrust component of displacement (Figure 5a). This Fault at the central part of the study area (Figure 6 and 7(C)) trends NE-SW with a depth range of about 300 m, the Fault occurs close to the contact between quartzite and migmatite. It formed a narrow band that indicates a sharp contrast between the magnetic low and magnetic high anomalies along profile ¹A and A. This linear narrow band with anomalous high magnetic signature (Figure 5a and 7(C)) signifies a brittle deformation with possible migration and deposition of magnetic minerals within the fault. The narrow zone coincides with a narrow stream channel and the prominent abrupt displacement of approximately 10 km low magnetic units to the north and south by a high magnetic unit at the centre of the map (Figure 5a). The displaced magnetic unit in the south appears to be rotated E-W, while the northern unit follows the prominent NNE-SSW direction. Fold 1 in Figure 6a, occur in the southwest part of the study area map, with the limbs dipping in the same direction, the axial plane is sub-horizontal. A recumbent fold is inferred.

Fold 2 (Figure 6a) occurs in the Northwest of the study area with its limb dipping in opposite directions which can be described as an inclined fold structure and also has a non-vertical axial plane. Fold 3 occurs in the northwestern part of the map, it has its limbs dipping in the opposite direction. Fold 4 occurs in the southwestern region of the study map, a little distance away from Fold 1 and its limbs are dipping in the same direction with its axial plane trending in the NE-SW direction. Fold 5 (Figure 6a) is situated close to the southern region of the map and the limbs are dipping in the opposite direction, the axial plane is inclined. It can be inferred that the fold is a close fold based on the angle between the fold limbs. Fold 6 is located in the Southeast region of the map and only one limb is captured in our map. Fold 7 is located in the north-central part of the map based on the angle between the limbs of the fold, it is a tight fold. Fold 8 is the main fold indicated on the map, the axial plane is oriented NNE-SSW (parallel to the Okemesi mega fold and the Ifewara Shear zone (Figure 1a), the limbs are dipping in the same direction and the western limb coincides with an inferred fault plane. Apart from Fold 1 and Fold 6 which are recumbent folds all the other folds have their axial surface and limbs in the same direction and can be interpreted as isoclinal folds. The limbs of these folds are parallel to each other and are tight in most cases, indicative of a compressional regime. Refolding of the earlier recumbent fold to form F₂ is evident in the F1 fold. The new f₂ fold is upright and open with a N-S axial plane, similar to the nappe structure in Ibadan area

(further southwest of map 1b in Fig 1). The rivers in the area explore the weak channels created by these structures, the river flows right through through the nose of the fold to the centre of the fold and downwards. While some of the rivers flows N-S in the direction of the refolded axial plane.

The study area lies within the south-eastern part of the Ifewara Shear Zone (Figure 1d). This shear zone was formed due to shearing activities of late Precambrian times (Odeyemi 1993). Deformation in this area is mainly controlled by the buckling and stretching of the competent metasedimentary layers. The quartzite rocks in the area under investigation are part of a long D₃ ductily deformed ridge. The shortening indicates a N-S transpression, classified as part of the early D₃ ductile deformation. The NNE-SSW trend is parallel to the Ifewara fault in the northwest. The first deformational episode is represented by a tight to close E-W to ENE-WSW trending recumbent fold (Figure 6 (Fold 1)), while the second deformational episode (D₂) is marked by the development of axial planar S₂ foliation trend that is subparallel to F₂. The third deformational episode (D₃) is marked partly by ductal deformation and later brittle deformation that resulted in the formation of both normal and strike slip faults. D₃ occur with prominent NNE-SSW to ENE -WSW trends which is the current dominant structural trend and tectonics in this area. Several of the folds (F2, F3, F4, F5, F7 (tight to isoclinal fold), while the F8 is isoclinal, open and symmetric with largest curvature is at the hinge line.

The reverse displacement and NE-SW trend of the major fault in this area are indicative of a dominant compressive regime and early D₃ deformation (Figure 7C).

The interpreted subsurface structural maps (Figure 6 and 7) were superimposed on the geologic map containing all the features with their respective depth estimates (Figure). This is to determine the relationship between the structures, lithology and associated mineralization. This will also help in determining the auspicious mineralization targets. The area indicates a predominantly compressive deformation with the development of folds, shear zones, curvilinear structures and a major reverse fault. Most of the identified folds are parallel to the main fault. The comprehensive information about the structural disposition in the area and the knowledge of the pre-existing geology of the area has helped in updating the geologic map of the study area. It can be inferred from the contacts C1, C2, C3, C5, and C6 that the contacts are

continuous and mostly NE-SW trending except in the southern part. It can also be inferred from the structural map that a major shear zone occurs within the migmatite region of the map close to the contact between the migmatite and the quartzite.

Conclusion

Application of selected filtering methods to the magnetic data, including reduction to the equator, horizontal and second vertical gradients, revealed five broad zones of NNE-SSW to NE-SE magnetic anomalies which could be correlated with identified structures. Positive magnetic residuals were associated with migmatite and granite-gneiss while negative magnetic residuals were associated with quartzites. The structural index maps which are the Euler deconvolution maps helped in the depth estimation of the structures. A subsurface geologic map was generated based on the geometry of the lithologic units at depth and on the comprehensive knowledge obtained about the lithologic and structural settings of the area. The major orientation of the structures is in the NNE-SSW to NE-SW direction and thus represents the main structural grain at depth. The major fault zone and fold zones are labelled fold one to eight with their orientation predominantly in the NNE-SSW to NE-SW direction, six contacts are denoted as C1-C6 with their orientation in the NNE-SSW to NE-SW direction. The recumbent folds with nearly horizontal limbs with almost E-W axial plane orientation (Fold 1 and Fold 6) and the NNE-SSW trends inferred in this interpretation belong to the first deformation episode (D1) while the NE-SW trending structures belong to the second deformation episode (D2). NE-SW oriented axial planes were possibly formed during the earlier ductile period of the D₃ deformational episode. The presence of folds in the area indicates that the area has suffered some episodes of ductile deformations. The subsurface structural trend coincides with the surface structural grain thus indicating that these structures are deep-seated or basement structures that extend to the surface.

Mineralization in most parts of the study area has been linked with structures. Further investigations should be carried out to establish the presence of economic minerals in this area. Economic minerals such as gold, tin and iron are being mined in Ijero-Ekiti and Aramoko-Ekiti (north of the study area (Figure 1a) with similar lithology and structure).

**The author declares no conflict of interest.
No funding was received for this research.**

References

- Akinlalu, A.A. (2023). Radiometric Mapping for The Identification of Hydrothermally Altered Zones Related to Gold Mineralization in Ife–Ilesa Schist Belt, Southwestern Nigeria. *Indonesian Journal of Earth Sciences*, 3(1), A 519. <https://doi.org/10.52562/injoes.2023.519>
- Ale, P.T., Dada, J.T. and Adewumi, A.J. (2014). Industrial Minerals potentials in Ekiti State SouthWestern Nigeria, *World Applied Sciences Journal* 29 (3) . 415 - 420. DOI:10.5829/idosi/wasj.2014.29.03.1544.
- Amigun, J.O. and Adelusi, A.O. (2013). Journal of Emerging Trends in Engineering and Applied Sciences, FUTA J. Res. Sci., Vol 9, No 2, pp. 225–234.
- Amigun, J.O., Afolabi, O. and Ako, B.D. (2012). Euler 3D deconvolution of analytical signal of magnetic anomalies over iron ore deposits in Okene, Nigeria; *Journal of Emerging Trends in Engineering and Applied Sciences*, pp. 711–717.
- Anifowose, A.Y.B. (2004). Remote sensing analysis of Ifewara-Zungeru Megalinear in Nigeria. PhD thesis, Federal University of Technology, Akure, Nigeria, 169p.
- Ariyibi, E.A. (2011). Integrated Geochemical and Geophysical Approach to Mineral Prospecting – A Case Study on the Basement Complex of Ilesa Area, Nigeria, *Advances in Data, Methods, Models and Their Applications in Geoscience*, Dr. Dong, Mei Chen (Ed.), ISBN: 978-953-307-737-6, *In Tech*, <http://www.intechopen.com/books/advances-in-data-methods-models-and-their-applications-in-geoscience/integrated-geochemical-and-geophysical-approach-to-mineral-prospecting-a-case-study-on-the-basement>
- Ariyibi, E.A. (2011). Integrated Geochemical and Geophysical Approach to Mineral Prospecting – A Case Study on the Basement Complex of Ilesa Area, Nigeria, *Advances in Data, Methods, Models and Their Applications in Geoscience*, Dr. Dong Mei Chen (Ed.), ISBN: 978-953-307-737-6, *In Tech*, Available . <http://www.intechopen.com/books/advances-in-data-methods-models-and-their-applications-in-geoscience/integrated-geochemical-and-geophysical-approach-to-mineral-prospecting-a-case-study-on-the-basement>
- Andongma, W.T., Gajere, J.N., Amuda, A.K., Edmond, R.R.D., Faisal, M. and Yusuf, D.Y. (2020). Mapping of hydrothermal alterations related to Gold mineralization within parts of the Malumfashi Schist Belt, North-Western Nigeria. *Egypt. J. Remote Sens. Sp. Sci.* 2021, 24, 401–417. Bellier, Olivier & Dumont, Jean & Sébrier, Michel & Jacques, And & Mercier, Jacques. (1991). Geological constraints on the kinematics and fault-plane solution of the Quiches Fault Zone reactivated during the 10 November 1946 Ancash earthquake, northern Peru. *Bull. seism. Soc. Am.* 81.
- Blakely, R.J. (1996). *Potential theory in gravity and magnetic applications*. Cambridge University Press, 441pp.
- Blakely, R.J. and Simpson, R.W. (1986). Approximating edges of source bodies from magnetic or gravity anomalies. *Geophysics*, 51(7), 1494–1498.
- Boesse, J.M. (1989). *A Geological Map of the Obafemi Awolowo University Campus*. Unpublished B. Sc. Thesis, Obafemi Awolowo University, Ile-Ife, Nigeria.
- Boesse, S. and Ocan, O. (1992). Geology and evolution of the Ife-Ilesha Schist belt, southwestern Nigeria. In *Benin-Nigeria Geotraverse. International Meeting on the Proterozoic Geology and Tectonics of High Grade Terrain*. IGCP 215, pp. 123-129.
- Fagbohun, B.J., Omitogun, A.A., Bamisaiye, O.A. and Ayoola, F.J. (2020). Remote Detection and Interpretation of Structural Style of the Zuru Schist Belt, Northwest Nigeria. *Geocarto International*, 1 – 16. doi:10.1080/10106049.2020.175382
- Grove, D.I., Goldfarb, R.J., Robert, F. and Hart, C.J.R. (2003). *Gold Deposits in Metamorphic Belts: Overview of current Understanding, Outstanding Problems, Future Research, and Exploration Significance*. *Economic Geology* 98 (1). pp1-29.
- Hassanein, H.I.E. and Soliman, K.S. (2008). Aeromagnetic Data Interpretation of Wadi Hawashiya Area for Identifying surface and subsurface structures, Northeastern Desert, Egypt.
- Ibraheem, I.M. (2019). Aeromagnetic Data: A Case Study of Sohag Area, Egypt *Geosc.* 9(5), BASEL.MDPI. ISSN 2076-3263
- Ishola, K.S., Akerele, P.O., Folarin, O., Adeoti, L., Adegbola, R.B. and Adeogun, O.Y. (2020). Application of aeromagnetic data to map subsurface structural features I Ewekoro, Southwestern Nigeria. *Model, Earth Syst. Environ.* 6, 2291-2302 <https://doi.org/10.1007/s40808-020-00812-y>.

- Kearey, P., Brooks, M. and Hill, I. (2003). An Introduction to Geophysical Exploration, 3rd Edition. Blackwell Science.
- Kolawole, F. and Anifowose, A.Y.B. (2011). Remote Sensing Analysis of a Dextral Discontinuity along Ifewara-Zungeru Area, Nigeria, West Africa. *Indian Journal of Science and Technology*. 4(1): 46–51.
- Ndougsa-Mbarga, T., Feumoe, A.N.S., Manguelle-Dicoum, E. and Fairhead, J.D. (2012). Aeromagnetic Data Interpretation to Locate Buried Faults in South-East Cameroon *Geophysical*, 48(1–2), 49–63.
- Nguimatsia, D.F.W., Bolarinwa, A.T., Yongue, R.F., de Dieu Ndikumana, J., Olajide-Kayode, J.O., Olisa, O.G., Abdu-Salam, M.O., Kanga, M.A. and Djou, E.S. (2017). Diversity of Gold Deposits, Geodynamics and Conditions of Formation: A Perspective View. *Open Journal of Geology*, 7, 1 6 9 0 - 1 7 0 9 . <https://doi.org/10.4236/ojg.2017.711113>
- Nwokeabia, C.N., Iduma, U., Ibe, S.O. and Bayelsa, O. (2018). Evaluating the economic potential of part of Ife-Ilesha schist Belt, Western Nigeria, using airborne magnetic and radiometric dataset. *IOSR Journal of Applied Geology and Geophysics*. 6(4):54-75.
- Odeyemi, I.B. (1985). Geological map of Ife-Ilesha schist belt. Unpublished
- Odeyemi, I.B. (1993). A comparative Study of remote sensing images of the structure of the Okemesi fold belt, Nigeria. *ITC Journal*, 1931-1, 77-81.
- Odeyemi, I.B., Anifowose, Y.B. and Asiwaju-Bello, Y.A. (1999). Multitechnique graphical analyses of fractures from remote sensing images of basement regions of Nigeria. *Journal of Mining and Geology*, 35 (1): 9-21.
- Onyedim, G.C. and Ocan, O.O. (2009). Spatial periodicities of structural features of the basement complex of southwestern Nigeria deduced from auto-covariance and power spectra of aeromagnetic data. *The pacific journal of science and Technology*. *Pac. J. Sci. Technol.* 10(1):556–566.
- Oyinloye, A.O. (2002b). Geochemical characteristics of some granite gneisses in Ilesha area southwestern Nigeria: implication on evolution of Ilesha schist belt, southwestern Nigeria. *Trends in Geochemistry India*. 2:59–71.
- Oyeniya, T.O., Salami, A.A. and Ojo, Samuel, B. (2022). Oyeniya, *et al* SOFT COPY.pdf. figshare. *Journal contribution*. <https://doi.org/10.6084/m9.figshare.19111898.v1>
- Rahaman, M.A. (1976). Review of the Basement Geology of Southwestern Nigeria in *Geology of Nigeria*, Elizabethan, Lagos, Nigeria. 564 p.
- Rahaman, M.A. (1988). Recent advances in the study of the basement complex of Nigeria; A publication of the Geological Survey of Nigeria, pp. 11–43.
- Rahaman, M.A. and Oyawoye, O. (1975). The Identified Lithology Units in Southwestern Nigeria. A publication of the Geological Survey of Nigeria, pp. 11–43.
- Reid, A.B., Allsop, J.M., Granser, H., Millet, A.J. and Somerton, I.W. (1990). Magnetic interpretation in 3-D using Euler deconvolution: *Geophysics*, 55, 80-91.
- Ugbor, C.C., Arinze, I.J. and Emedo, C.O. (2020). Analysis of Aeromagnetic Data of Ikwo and Environs, Southeastern Nigeria: A mineral and Hydrocarbon Exploration Guide. *Nat Resource Res* 29 . 2 9 1 5 - 2 9 3 2 . <https://doi.org/10.1007/s11053-020-09633-3>.
- Wen, I.J. and Bevis, M. (1987). Computing the gravitational and magnetic anomalies due to a polygon: algorithms and Fortran subroutines. *Geophysics*, 52, 232–238.
- Zhang, J., Zeng, Z., Zhao, X., Li, J., Zhou, Y. and Gong, M. (2020). Deep Mineral Exploration of the Jinchuan Cu-Ni Sulfide Deposit Based on Aeromagnetic, Gravity, and CSAMT Methods. *Minerals*, Vol. 10 (2). doi:10.3390/min1020168.



GARNET ENERGY SERVICES NIGERIA LTD.

Geological, Petroleum and Environmental Consultants

12 Floor, Bookshop House, 50/52 Broad Street, Lagos
P.O. Box 70011, Victoria Island, Lagos, Nigeria
Tel. 01-8546699, 06035101804
E-mail mariesonuga@yahoo.com



BARACAL CONSULT LTD.

Environmental Consultants

Suite 65/66 Dolphin Plaza, Dolphin Estate, Ikoyi
P.O. Box 70885, Victoria Island, Lagos, Nigeria
Tel. 234-1-7741441, 234-1-2629251 Fax 234-1-2610735
E-mail baracalnig@yahoo.com, carolsoladg@yahoo.com



Jonakod Nigeria Limited

Energy, Environment & Safety Consultants

34 Ontario Crescent, Maitama, Abuja
Tel. 09-4133521, 08035300958, 08057467878
E-mail jonas_odocha@yahoo.com



AMJU SERVICES NIG. LTD.

Specialists in Geological & Mining Services

1B Rock Road, Off Rabah Road
P.O. Box 7216, Kaduna, Nigeria
Tel. +234-(0)8054073338
E-mail abuykarofi@gmail.com
